THE JOURNAL OF BIOLOGICAL CHEMISTRY VOL. 290, NO. 8, pp. 4590–4603, February 20, 2015

CD36 Binds Oxidized Low Density Lipoprotein (LDL) in a Mechanism Dependent upon Fatty Acid Binding*

Received for publication, November 20, 2014, and in revised form, December 24, 2014 Published, JBC Papers in Press, January 1, 2015, DOI 10.1074/jbc.M114.627026

Anthony G. Jay[‡§], **Alexander N. Chen**[§], **Miguel A. Paz**[§], **Justin P. Hung**[§], **and James A. Hamilton**[§1]

From the Departments of [‡]*Biochemistry and* [§]*Physiology and Biophysics, Boston University, Boston, Massachusetts 02118*

Background: CD36 is expressed in many cell types and binds diverse ligands including oxidized LDL (oxLDL) and unesterified fatty acid (FA).
Results: FA bind to CD36, which leads to oxLDL binding and uptake independent of CD36 disulfide bonds.
Conclusion: Typical dietary FA enhance uptake of oxLDL.
Significance: This study provides a possible mechanism for oxLDL binding CD36 that is dependent upon specific FA types.

The association of unesterified fatty acid (FA) with the scavenger receptor CD36 has been actively researched, with focuses on FA and oxidized low density lipoprotein (oxLDL) uptake. CD36 has been shown to bind FA, but this interaction has been poorly characterized to date. To gain new insights into the physiological relevance of binding of FA to CD36, we characterized FA binding to the ectodomain of CD36 by the biophysical method surface plasmon resonance. Five structurally distinct FAs (saturated, monounsaturated (*cis* and *trans*), polyunsaturated, and oxidized) were pulsed across surface plasmon resonance channels, generating association and dissociation binding curves. Except for the oxidized FA HODE, all FAs bound to CD36, with rapid association and dissociation kinetics similar to HSA. Next, to elucidate the role that each FA might play in CD36-mediated oxLDL uptake, we used a fluorescent oxLDL (Dii-oxLDL) live cell assay with confocal microscopy imaging. CD36-mediated uptake in serum-free medium was very low but greatly increased when serum was present. The addition of exogenous FA in serum-free medium increased oxLDL binding and uptake to levels found with serum and affected CD36 plasma membrane distribution. Binding/uptake of oxLDL was dependent upon the FA dose, except for docosahexaenoic acid, which exhibited binding to CD36 but did not activate the uptake of oxLDL. HODE also did not affect oxLDL uptake. High affinity FA binding to CD36 and the effects of each FA on oxLDL uptake have important implications for protein conformation, binding of other ligands, functional properties of CD36, and high plasma FA levels in obesity and type 2 diabetes.

The scavenger receptor family, which includes CD36, has expanded to encompass eight different subclasses of structurally unrelated receptors that, under the classical definition, share the defining feature of binding modified forms of LDL (1, 2). The uptake of modified lipoproteins by scavenger receptors is thought to be central to foam cell formation and is widely believed to represent one of the major activation events stimulating the proinflammatory phenotype of lesional macrophages (1, 3, 4). Furthermore, scavenger receptors initiate signaling cascades that regulate macrophage activation, lipid metabolism, and inflammatory programs that may influence the development and stability of atherosclerotic plaques (5, 6). CD36 is a prominent member of the scavenger receptor family in part because of its robust catalysis of oxLDL[2] uptake and the CD36-specific atheroinflammatory signaling connected to these events (4). Furthermore, its expression in cells is associated with cardiovascular disease, which includes surface expression on platelets, adipocytes, skeletal and cardiac myocytes, capillary endothelial cells, most professional phagocytes, and epithelial cells in gut, kidney, and breast (7). The physiological relevance of oxLDL has been questioned and also debated. Despite mixed results from various randomized controlled trials using antioxidant therapy to treat oxLDL, 14 clinical cohort studies have demonstrated an association between oxLDL measurement and cardiovascular events (8). Furthermore, specifically CD36 and oxLDL levels have recently been shown to be associated with cardiovascular risk factors in young subjects (4).

CD36 binds oxLDL with an affinity as high as or higher than any other currently examined scavenger receptor family members (9, 10). Early studies illustrated the significant role of CD36 in binding/uptake of oxLDL based upon a genetic polymorphism in the CD36 gene identified in Japanese subjects shown to result in deficient expression of CD36 (the NAK^{a-} phenotype) (11). Monocyte-derived macrophages isolated from these patients were seen to bind ~40% less oxLDL and accumulate ~40% less cholesteryl ester from oxLDL than cells derived from normal controls (12). The site of this oxLDL binding to CD36 has been identified and recently mapped to amino acids 157–171, with critical lysines at positions 164 and 166 (13–15). This is consistent with the pH profile and salt concentration dependence, which suggest an electrostatic contribution to the CD36-oxLDL binding (14). Additionally, CD36 is part of the conserved scavenger receptor cysteine-rich superfamily characterized by the presence of one

* This work was supported by the American Diabetes Association Grant 1-11-BS-R62 (to J. A. H.).
[1] To whom correspondence should be addressed: Dept. of Physiology and Biophysics, Boston University, 700 Albany St, W302, Boston, MA 02118. Tel.: 617-638-5048; E-mail: jhamilt@gmail.com.

[2] The abbreviations used are: oxLDL, oxidized LDL; FA, fatty acid; DHA, docosahexaenoic acid; SPR, surface plasmon resonance; SSO, sulfo-*N*-hydroxysuccinimidyl ester of oleate; OA, oleic acid; EA, elaidic acid; HODE, 9*S*-hydroxy-10*E*,12*Z*-octadecadienoic acid; TCEP, tris(2-carboxyethyl)phosphine; DPBS, Dulbecco's PBS; MβCD, methyl-β-cyclodextrin; RU, resonance units; HSA, human serum albumin; Ni-NTA, nickel-nitrilotriacetic acid.

or several repeats of an ancient and highly conserved protein module (16). The three characterized disulfide bonds in the ectodomain of CD36 (17) are active in CD36-mediated cytoadherence of *Plasmodium falciparum* (malaria)-infected red blood cells (18), indicating potential oxLDL binding to CD36 through disulfide bonds and treatment strategies using reducing strategies such as targeted nanodrugs.

Although the best characterized function of CD36 is to bind and internalize oxLDL, another widely studied role of CD36 is in direct binding of FA (19) and in augmenting FA uptake (20–22). We have recently shown that CD36 increases FA uptake through intracellular esterification but does not increase mass transport of FA across the plasma membrane, transport that occurs within seconds in cells with or without CD36 (21). This raises questions regarding the mechanism and role of FA binding to CD36.

Initial studies, conducted using the probe sulfo-*N*-hydroxysuccinimidyl ester of oleate (SSO) and the FA derivative isopropyl myristate, showed apparent inhibition of adipocyte FA uptake, and a subsequent study showed that radiolabeled SSO bound covalently to CD36 (23, 24). CD36 was shown to have a significant homology to M-FABP throughout 73% of its sequence, suggesting that a FA binding region was present in the extracellular domain, yet the only reported study of natural FA showed very weak binding to CD36 with apparent dissociation constants of ~1 μM (19). However, the approaches used had several technical limitations and showed FA to have similar low affinity for albumin, which has well characterized binding constants in the nanomolar range (25). Using SSO as a probe of FA binding, point mutations of CD36 appear to disrupt oxLDL binding to CD36 and inhibit FA uptake in CHO cells (23, 26). Furthermore, new studies have indicated that certain FAs inhibit oxLDL binding to synthetic CD36 peptide fragments (27, 28). Along with our recent findings, these new studies provide a strong rationale for applying new methods to better characterize FA binding to CD36.

In this study, we applied and optimized a new methodology to study CD36 binding of various label-free FA from five structural groups (oleic acid (OA), elaidic acid (*trans*-oleic acid; EA), 9*S*-hydroxy-10*E*,12*Z*-octadecadienoic acid (oxidized linoleic acid commonly found in oxLDL (29); HODE), palmitic acid (PA), and docosahexaenoic acid (DHA)). Our chosen method, surface plasmon resonance (SPR), provided quantitative information about affinity, specificity, and kinetics. Next, we sought to provide insight into molecular mechanisms for the binding of CD36 with oxLDL together with each of the above FA, by investigating Dii-oxLDL uptake using a fluoresence binding/uptake assay and confocal microscopy. Our findings support the proposed electrostatic mechanism of CD36 binding of oxLDL, along with FA acyl chain contributions. Finally, we have shown that binding of CD36 to oxLDL is independent of the CD36 disulfide bonds using DTT and tris(2-carboxyethyl) phosphine (TCEP) reductions.

EXPERIMENTAL PROCEDURES

Cell Culture and DNA Transfection—For all cell culture experiments, low passage number cells were used, purchased from ATCC (Manassas, VA). The cells were grown at 37 °C and 5% CO_2 in phenol-free, low glucose (5 mM) DMEM (Invitrogen) supplemented with 10% heat-inactivated FBS (Invitrogen) and 1% penicillin/streptomycin. DNA transfections were done using Lipofectamine2000 (Invitrogen) diluted into unsupplemented Opti-MEM (Invitrogen) using either HeLa cells or human embryonic kidney cells (HEK293) grown to ~80% confluence in 60-mm dishes. All DNA used had the same vector backbone (pCI-neo-empty or pCI-neo-CD36), and expression levels and localization were previously verified using Western blotting, microscopy, and fractionation as published (21), except pcDNA3.1-EGFP-CD36, in which CD36 was cloned into a pcDNA3.1-EGFP (pcDNA-3.1 enhanced green fluorescent protein) plasmid (Invitrogen). DNA used in transfections had a final concentration at 0.8 μg each DNA per 60-mm dish. All experiments using transfected cells were performed within a 5-day period from day 1 of transfection to maximize protein expression.

Immunofluorescence Staining with Dii-oxLDL and Confocal Microscopy—For Dii-oxLDL uptake experiments, HEK293 cells were grown in 8-well BD Falcon™ culture slides (Franklin Lakes, NJ) to ~60% confluence. Dii-oxLDL (1,1′-dioctadecyl-3,3,3′,3′-tetramethylindocarbocyanine perchlorate) from LDL isolated from human plasma and oxidized via copper sulfate oxidation and then analyzed for the degree of oxidation using the thiobarbituric acid reactive substances (TBARS) assay and migration *versus* native LDL on agarose gel electrophoresis was purchased from Biomedical Technologies Inc. (Stoughton, MA). Dii-oxLDL was also stored at 4 °C unfrozen and used fresh within 2 weeks of receiving, per manufacturer's instructions, and was premixed at 5 μg/ml into DMEM with 10% FBS, or DMEM with 10% charcoal-stripped FBS (Sigma, catalog no. F6765), or serum-free DMEM with added FA (OA, EA, HODE, PA, and DHA). For metabolic studies, the acyl CoA synthetase inhibitor triacsin C (Enzo Life Sciences, Farmingdale, NY) was additionally added at a final concentration of 24 μM as our lab has done previously (30). Prior to being added, all FA was solubilized into Dulbecco's PBS (DPBS) with methyl-β-cyclodextrin (MβCD) at molar ratios of 1 FA:6 MβCD for OA, EA, and HODE and 1 PA:12 MβCD and 1 DHA:1 MβCD. Into each cell culture well, 200 μl/well of media was added for 90 min at 37 °C. All steps after this point were completed under darkness. After Dii-oxLDL incubation, the cells were washed twice in warm DPBS + 0.1% Tween 20 and 1% BSA and then fixed with 4% paraformaldehyde in DPBS at room temperature for 10 min. The cells were washed again with DPBS once, permeabilized with 0.1% Triton X-100 in DPBS, washed twice in DPBS, and blocked in 10% BSA in DPBS for 1 h at room temperature. This blocking was followed by overnight 4 °C incubation with monoclonal rabbit anti-CD36 primary antibody (EPR6573, Abcam) or monoclonal mouse anti-CD36 primary antibody (JC63.1, Abcam) at a dilution of 1:100. The cells were then washed three times for 5 min in DPBS buffer and then incubated with Alexa Fluor® 488 goat anti-rabbit IgG antibody (Invitrogen, catalog no. A-11008) or Alexa Fluor® 488 goat anti-mouse IgG antibody (Invitrogen, catalog no. A-11001) for 1 h at room temperature. After washing with DPBS three times for 5 min, the cells were mounted with ProLong® Gold antifade reagent containing DAPI (Invitrogen, catalog no. P-36931) and a #1 glass cover slide. The stained cells, including three-dimensional z-stack images, were photographed using an Olympus DSU

Spinning Disk Confocal microscope (Center Valley, PA) using CellSens Acquisition Software, maintaining the gain and exposure settings between each channel for all images. Red Dii-oxLDL fluorescence was quantified by opening only the red channel images in ImageJ (National Institutes of Health, Bethesda, MD), subtracting background, and using Analyze/Measure to get a total red fluorescence value. This number was normalized by dividing it by the total cell number, obtained by converting the DAPI nuclear channel image to binary format and using the Image-based Tool for Counting Nuclei plugin (31).

Surface Plasmon Resonance Analysis—Using the ProteOn XPR36 protein interaction array system (Bio-Rad) (32), all experiments were performed in high salt PBS (200 mM, pH 7.4) running buffer to decrease nonspecific binding, with or without 5 mM MβCD to dissociate FA, at a flow rate of 30 μl/min at 25 °C. ProteOn GLM chips were chosen for the experiment after our first initial trials with GLC chips did not give sufficient signal response. All six channels (GLM sensor chip), including the empty well used to normalize nonspecific binding, were activated for 5 min with a mixture of 0.2 M 1-ethyl-3-(3-dimethylaminopropyl)carbodiimide hydrochloride and 0.05 M sulfo-*N*-hydroxysuccinimide. Immediately after activation of the surfaces, proteins were added for covalent linking. Channel 1 was used as a reference. For the negative control, normal rabbit IgG (Cell Signaling Inc., Danvers, MA, catalog no. 2729) was diluted into 10 mM sodium acetate buffer, pH 4.5, at 300 μl/well. Using 0.25 mg/ml normal rabbit IgG stock solution, 5 μl/well yielded ~1,300 resonance units (RU), injected across channel 2. Recombinant ectodomain of human CD36 (rCD36) from amino acids 30–439, *i.e.* lacking both the transmembrane and the small intracellular domains (Sino Biologicals Inc., Daxing, China), was diluted into 4:1 PBS:10 mM sodium acetate buffer, pH 4.5 (Bio-Rad) at 300 μl per/well. PBS was used because the theoretical isoelectric point of CD36 is 8.19 (ExPASy). Experimentally it was found that using 0.25 mg/ml rCD36 stock solution at 3 μl/well yielded ~1,300 RU, and 12 μl/well yielded ~5,000 RU in channels 3 and 4, respectively. For a positive control, human serum albumin (HSA, Sigma-Aldrich, catalog no. A3782) was diluted into acetate buffer, pH 4.5, at 300 μl/well. Using 0.25 μg/ml HSA stock solution, experimentally adding 5 μl/well yielded ~1,300 RU and 10 μl/well yielded ~5,000 RU in channels 5 and 6, respectively. Finally, after protein linkage, all six channels were blocked with 1 M ethanolamine HCl (pH 8.5).

Various FA were then injected into channels perpendicular to ligands, at six different concentrations, using a 2-fold dilution series within a variable range, dependent upon experimental FA R_{max}, which differed for each individual FA tested. In additional experiments, Dii-oxLDL was injected at doses of 1, 4, and 8 nM, with or without 150 μM OA, using an assigned and approximate molecular mass value for Dii-oxLDL at 3,000,000 g/mol. In these assays, Dii-oxLDL molecular mass was assigned at 3 million daltons (34) for the purpose of Langmuir modeling. The six concentrations were injected simultaneously at a flow rate of 200 μl/min at 25 °C, unless otherwise noted. The GLM sensor chip was regenerated with short injection of 1 M NaCl between consecutive FA measurements. For Dii-oxLDL regeneration, three separate injections of glycine buffer (pH 3.0), 0.5% SDS, and 1 M NaCl, respectively, were used. The results are expressed in arbitrary RU with subtraction of RU values from channel 1. The data were analyzed with ProteOn Manager™ software, using the Langmuir model (A + B [dharrow] AB) for fitting kinetic data. For each FA, as well as for all Dii-oxLDL SPR experiments, a set of five separate experiments were performed and analyzed. Error bars were not included for visual clarity but were $<\pm 25$ RU for each experiment set.

In Vitro Solid Phase CD36 and Dii-oxLDL Binding Assay—CD36 and Dii-oxLDL binding was measured using slight modifications to previously published work (35, 36), such as the use of *n*-dodecyl-β-D-maltoside (ThermoScientific) in place of octyl β-D-glucoside. In brief, rCD36-His_6 purified from HEK293 cells lacking both the transmembrane and the small intracellular domains (Sino Biologicals Inc., Daxing, China) was added at 1 μg/well of a 96-well Ni-NTA-coated HisSorb™ plate (Qiagen) as a 100-μl aliquot in protein binding buffer (20 mM Tris-HCl, pH 6.8, 150 mM NaCl, 1.5 mM $MgCl_2$, 5% (v/v) glycerol, 0.5% (w/v) *n*-dodecyl-β-D-maltoside) and bound overnight at 4 °C with gentle rocking. Unbound protein was aspirated, and each well was washed with 2 × 200 μl of room temperature ligand binding buffer (PBS, 1 mM $MgCl_2$, 1 mM $CaCl_2$, 0.5% (w/v) *n*-dodecyl-β-D-maltoside, 0.2% (w/v) fatty acid-free BSA). After this wash, 10 mM DTT (ThermoScientific) or 10 mM TCEP (ThermoScientific) were added in ligand binding buffer, to select wells, for 5 min at room temperature with gentle rocking and then removed by aspiration. Dii-oxLDL was then added in ligand binding buffer (± 10 mM DTT or 10 mM TCEP) in a total assay volume of 100 μl. The binding reaction was incubated for 90 min at room temperature, with gentle rocking. Unbound ligand was removed, and the wells were washed three times with 150 μl of ice-cold wash buffer (PBS, 1 mM $MgCl_2$, 0.05% BSA). PBS (50 μl) was added per well prior to determining the amount of bound fluorescence using a fluorescence plate reader (Infinite M1000 PRO, Tecan; excitation, 514 nm; emission, 550 nm). Specific binding of Dii-oxLDL was calculated after subtraction of the level of Dii-oxLDL bound nonspecifically to empty wells.

The data from all binding assays were analyzed using OriginLab version 8.6 software. Saturation binding data that showed saturable binding of ligand to CD36 over a range of ligand concentrations were best fitted by the Langmuir adsorption isotherm, shown in Equation 1, which describes binding of ligand to a single class of binding site,

$$B = \frac{B_{max} \times [L]}{K_d + [L]} \quad \text{(Eq. 1)}$$

where B is bound ligand (relative fluorescence units), B_{max} is maximal binding (relative fluorescence units), $[L]$ is concentrations of ligand (μg/ml), and K_d is the concentration of ligand (μg/ml) giving half-maximal binding and is a measure of the affinity of the receptor-ligand interaction.

RESULTS

CD36 Binds Oleic Acid with Comparable Kinetic On/Off Rates to Albumin but with Decreased Affinity and/or Binding Sites—To study the binding of CD36 to natural FA without potentially perturbing labels, we applied a new methodology

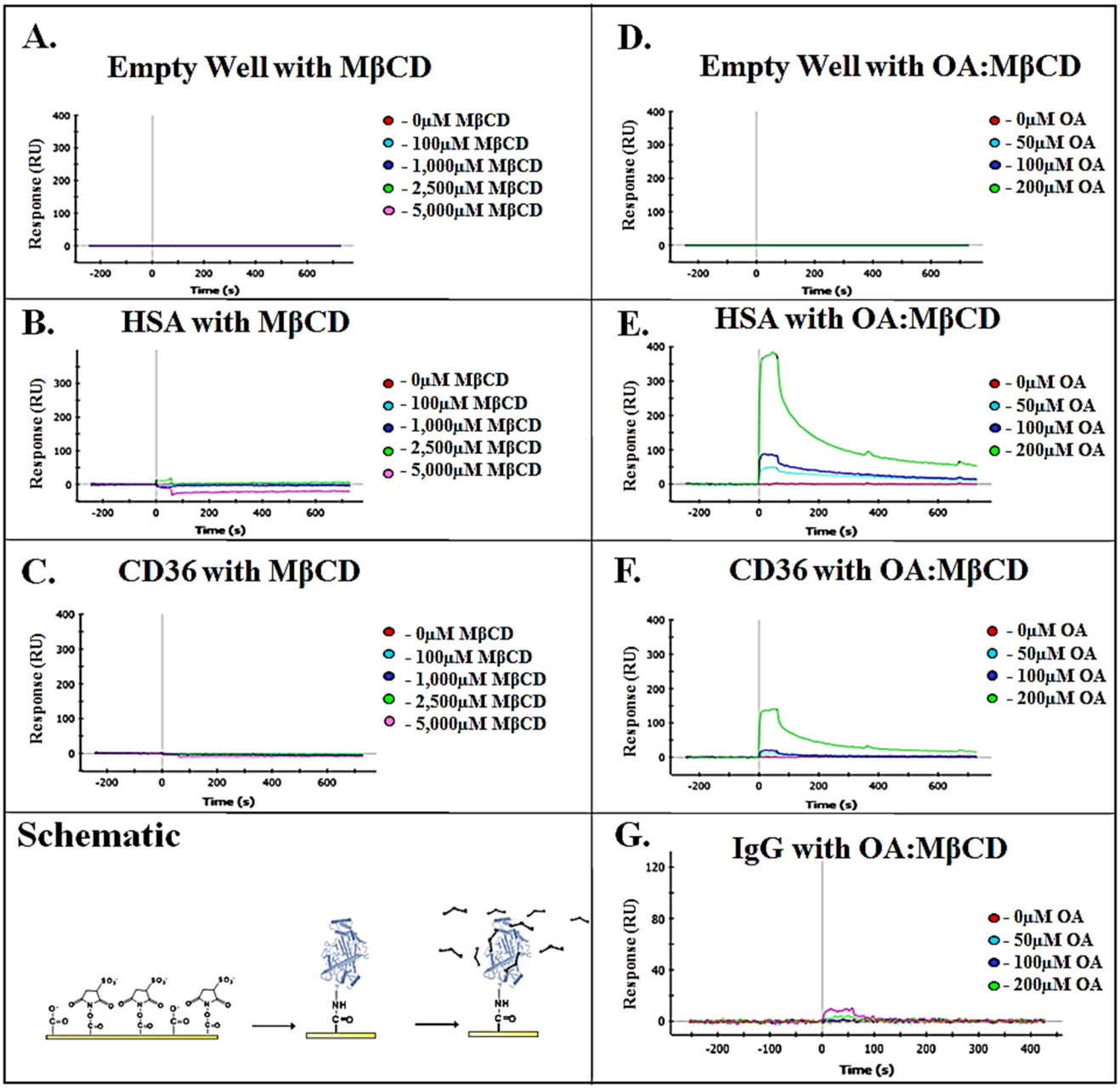

FIGURE 1. *A* and *D*, 1-ethyl-3-(3-dimethylaminopropyl)carbodiimide hydrochloride/*N*-hydroxysuccinimidyl activated and ethanolamine quenched empty lanes from a single 6-well Bio-Rad Proteon XPR36 GLM SPR chip, which have increasing concentrations of (*A*) MβCD and (*D*) 1 OA:6 MβCD pulsed across the surface, to correct for nonspecific empty lane binding. *B* and *C* are normalized to *A* and show HSA bound to the chip surface with only MβCD pulsed across (*B*) and CD36 bound to the chip surface with only MβCD pulsed across (*C*), in increasing doses. No significant binding of MβCD to CD36 or HSA were observed. *E*–*G* are normalized to *D* and show HSA (*E*), CD36 (*F*), or IgG (*G*) bound to the chip surface with OA:MβCD pulsed across, in increasing doses. Binding of OA is seen with HSA (*E*); $K_a = 1.0\ e^3$ 1/ms, $K_d = 7.9\ e^{-3}$ 1/s, and $K_D = 7.9\ e^{-6}$ M. Binding of OA is seen with CD36 (*F*); $K_a = 1.0\ e^3$ 1/ms, $K_d = 8.2\ e^{-3}$ 1/s, and $K_D = 8.2\ e^{-6}$ M. Although these numbers may not represent accurate K_D values, the relative value is important. Note that when higher amounts of OA were added with CD36, no higher signal was observed (data not shown). *G*, no significant binding of OA was observed with IgG bound to the chip. The *bottom left panel* illustrates an *N*-hydroxysuccinimidyl-activated SPR chip surface (*left part*) with CD36 mobilized by covalent linkage (*middle part*) and FA being pulsed through the flow channel containing CD36 (*right part*). The covalent linkage of CD36 is at amino acids 30 and 439 (full-length protein is 1–472), which is adjacent to the lipid bilayer in the full-length protein.

(SPR) and a novel approach to solubilize FA for this binding assay. Fully glycosylated recombinant CD36, purified from HEK293 cells without the TM domains, was linked to an SPR sensor chip surface, and various OA doses were pulsed across the chip surface to investigate the potential binding affinity and kinetics of the OA interaction with CD36 (Fig. 1, *Schematic*). Because this was a new experimental approach for CD36, we included extensive controls (Fig. 1, *B*, *C*, *E*, and *G*). In addition, the design of the experiment necessitated maintaining FA in a soluble form in high concentrations. To overcome solubility limitations and artifacts, we used MβCD as a delivery vehicle. Our lab has characterized the interactions of several FA with MβCD and demonstrated that in aqueous buffer, FAs dissociate from MβCD and partition into lipid bilayers within ms (37, 38). Additionally, FA:MβCD in PBS buffer is more physiologically relevant than typical organic solvents used to solubilize FA

(*e.g.* 100% DMSO). Organic solvents are also incompatible with SPR at high volume percentages because of their high refractive index leading to maximal SPR resonance units. In our SPR experiments, we tested up to 5 mM MβCD with CD36 linked to the SPR chip surface and saw no significant binding or dose dependence in these controls (Fig. 1, *A–C*).

For comparison with our CD36 results, we performed parallel experiments with HSA as a positive control. HSA was covalently linked to the SPR chip surface with the same RU amount bound as CD36 (experimentally determined, as described under "Experimental Procedures"; Fig. 1, *B* and *E*). We found that HSA bound and released OA rapidly and with a high RU response (for example, Fig. 1*E*), which was expected from extensive previous studies of FA binding, including those in our lab with albumin (39, 40) and FABP1 (41, 42). As an additional negative control, we bound IgG to the chip surface and saw no OA binding, as expected (Fig. 1*G*). Fig. 1*F* shows our SPR data for OA binding to CD36 binding with a dose-responsive RU response. There was a large RU increase between 100 and 200 μM, relative to the other OA doses, which was also seen in the positive control HSA. The upper range of RU saturation for CD36 was found at ~200 μM OA, and higher OA doses were found to not significantly increase RU signal beyond 200 μM OA concentrations (R_{max}).

Serum Is Required for Large Quantity CD36-mediated oxLDL Binding—Although our SPR experiment does not directly quantify the number of OA binding sites, the comparison of data for HSA (with nine known sites) and CD36 provides the first biophysical evidence for the presence of several binding sites on CD36. Most of the focus on interactions of CD36 with FA has been on binding of a single FA molecule to a site in the large ectodomain with structural homology FABP and how such binding could promote mass transport of FA through the plasma membrane (20, 43). FA binding (either one or several molecules) would not likely be sufficient binding for mass FA transport but could affect binding of LDL, especially with evidence that site-specific CD36 inhibitors have indicated that FA and oxLDL bind CD36 in the same peptide region (26). Consequently, we investigated the physiological significance of this FA binding using an established fluorescence-labeled oxLDL (Dii-oxLDL) binding/uptake assay. We first examined whether FA binding was a prerequisite for oxLDL binding by adding Dii-oxLDL to HEK293 cells expressing CD36 (pCI-neo-CD36) in either DMEM with 10% FBS, which contains a mixture of biological FA, or DMEM without serum (Fig. 2). HEK293 cells expressing empty vector control (pCI-neo-empty) were used as a negative control (Fig. 2, *u–x* and *C*).

As shown in Fig. 2 (*a–d*), robust binding of Dii-oxLDL occurred in the presence of serum, but very little binding was detected when serum was not present in the assay (Fig. 2, *e–h*). Additionally, when 10% FBS was used that had been charcoal-stripped of hydrophobic molecules (*i.e.* FA, hormones, etc.), the Dii-oxLDL binding was again nearly completely eliminated (Fig. 2, *i–l*). Because oxLDL purified from human plasma contains enough FA to affect LDL electronegativity (44), it is possible that the observed small amount of basal Dii-oxLDL binding may be accomplished through FA already present on oxLDL.

Oleic Acid Enhances CD36-mediated oxLDL Binding—FBS has been shown to contain a ratio of saturated, monounsaturated, and polyunsaturated FA (34.0, 34.3, and 27.8%, respectively), with almost 30% of the total FA composition being comprised of OA (45). Because SPR demonstrated that CD36 binds OA, we added OA to Dii-oxLDL in serum-free DMEM to HEK293 cells expressing CD36 (Fig. 2, *m–t*) or to empty control vector (Fig. 2, *u–x*). Not only was Dii-oxLDL binding rescued with OA added to the serum-free medium, the surface expression of CD36 was altered at higher doses of OA, and binding became even greater than with serum (Fig. 2, *q–t*, *A*, and *B*).

Having demonstrated binding of oxLDL to the surface receptor CD36 by microscopy, it is important to determine whether Dii-oxLDL was being internalized by the cells expressing CD36 (uptake) or whether Dii-oxLDL was only binding CD36 at the plasma membrane, where CD36 is predominantly localized in our HEK293 cell system (21). To discriminate these two possibilities, we expressed GFP-CD36 and used three-dimensional confocal microscopy to visualize the Dii-oxLDL location in the z-plane relative to CD36 localized at the cell surface and relative to the cell nuclei (Fig. 3, *A–C*). The merged image panel shows that most of the Dii-oxLDL bound by cells expressing GFP-CD36 (Fig. 3*C*, *yellow*) was internalized, indicating that binding to CD36 was followed by oxLDL uptake when OA is present, within the 90-min incubation. In addition, because we have recently shown that CD36 is involved in activating and therefore traps FA inside cells by enhancing esterification (21), we inhibited the first step of FA activation by using the acyl-CoA synthetase inhibitor, triacsin C, for the 90-min incubation of Dii-oxLDL and OA and found no significant difference with or without this inhibitor (see Fig. 5, *A–D*).

Next, to focus directly on FA effects of oxLDL binding to CD36, we performed additional *in vitro* SPR experiments in which Dii-oxLDL was pulsed across the SRP chip surface containing bound CD36 in the presence and absence of OA. Here we observed significantly more binding of Dii-oxLDL to CD36 when 150 μM OA was present along with Dii-oxLDL than with Dii-oxLDL alone and very little binding of oxLDL to the negative control, IgG (Fig. 3, *D–F*). For example, when 4 nM oxLDL by itself is pulsed across CD36, the RU of binding is ~130 (Fig. 3*E*, *green line*). When 4 nM oxLDL with 150 μM OA:MβCD is pulsed across CD36, ~400 RU of binding is observed (Fig. 3*F*, *green line*), even though OA:MβCD by itself only adds ~100 RU (*expected* RU of binding: 130 RU + 100 RU = 230 RU; *observed* = ~400 RU). This indicates that OA may be opening/facilitating an oxLDL binding site on CD36, to increase oxLDL binding. Furthermore, because human source oxLDL contains FA, it is possible that the FA present on oxLDL is enabling the binding to CD36 seen when additional OA is not added (Figs. 3*E* and 2, *e–l*). Experiments with FA-free oxLDL would need to be performed in future studies to determine whether this is the case.

The trans-Isomer of Oleic Acid (Elaidic Acid) Binds to CD36 and Increases Dii-oxLDL Uptake—The OA *trans*-isomer, EA, commonly formed by the partial hydrogenation of vegetable oils and commonly consumed by humans, also bound both CD36 and HSA but with slower and possibly biphasic kinetics of adsorption (Fig. 4, *A* and *E*). Along with each experiment

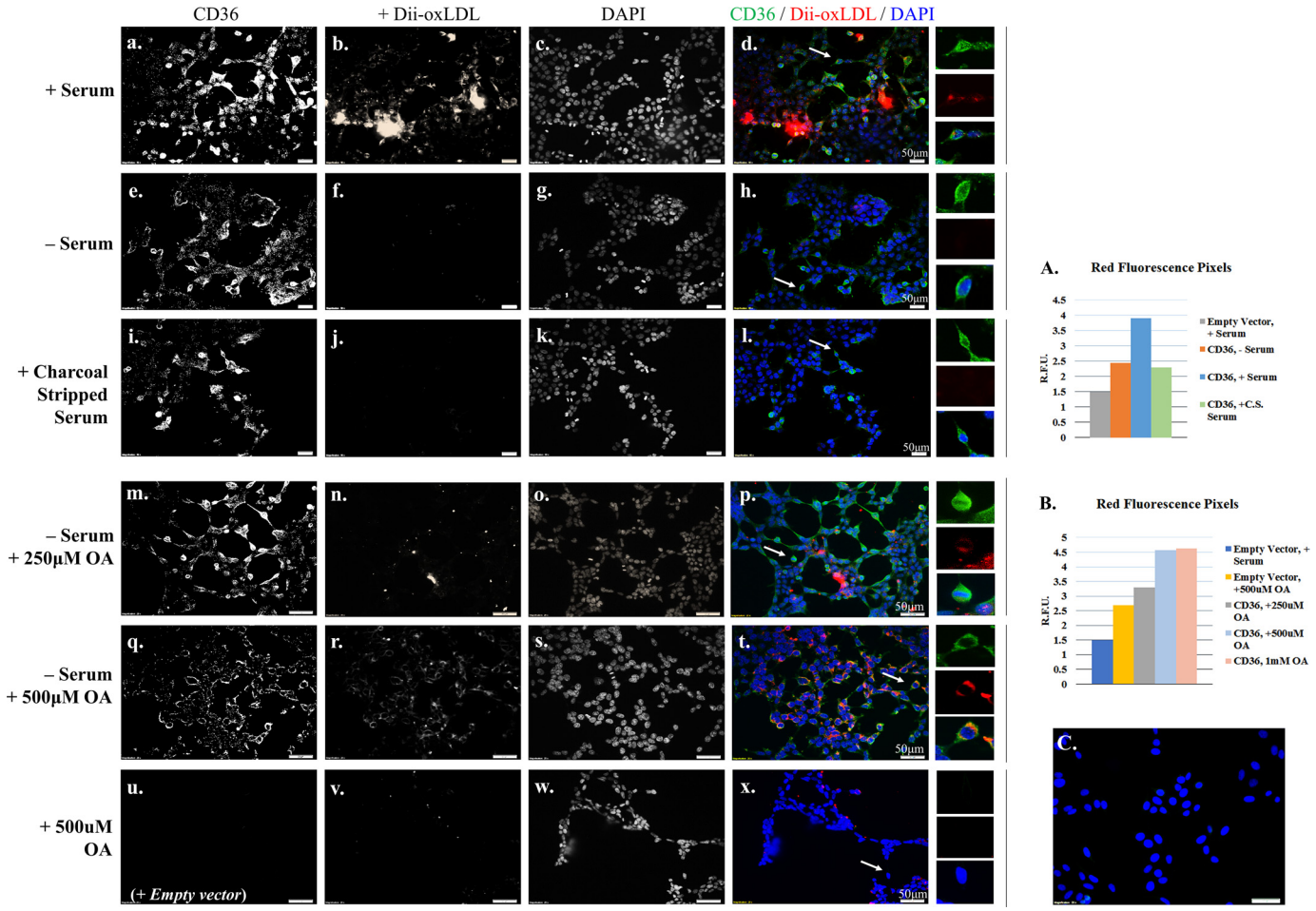

FIGURE 2. *Panels a–x*, merged 20× confocal micrographs of HEK293 cells, transfected with pCI-neo-CD36 (*panels a–t*) or pCI-neo-empty vector control (*panels u–x*), with 5 μg/ml Dii-oxLDL (shown in *red* in the merged image) added for 90 min at 37 °C in DMEM with 10% FBS (*panels a–d*), DMEM without serum (*panels e–h*), DMEM with 10% charcoal-stripped FBS (*panels i–l*), or serum-free DMEM with only OA added back (*panels m–x*). After Dii-oxLDL incubation, the cells were fixed and stained for CD36 (shown in *green* in the merged image) and the nuclear stain DAPI (shown in *blue* in the merged image). Under different conditions, CD36 surface distribution appears to change (*panels a*, *e*, *i*, *m*, and *q*) especially with or without serum (*panel a versus panel e*) or when increasing doses of OA were added (*panel m versus panel q*). *White arrows* in each merged image (*panels d*, *h*, *l*, *p*, *t*, and *x*) indicate representative enlarged cells in the original color scheme, shown on the *small right panels*. All OA added was complexed to MβCD (1 OA:6 MβCD), as in SPR experiments. *A* and *B* show quantification of (Dii-oxLDL) from Fig. 2 (*panels a–l*), after background subtractions, in a 20× magnified, 200-cell field (*A*) and quantification of red fluorescence pixels where doses of OA were added (*panels m–x*, 1 mM OA addition confocal images not shown) (*B*), where R_{max} is defined as ~500 μM. *C*, additional control merged confocal micrograph of HEK293 cells transfected with pCI-neo-empty control vector, with 5 μg/ml Dii-oxLDL (*red*) added for 90 min at 37 °C in DMEM with 10% FBS. The cells were then fixed and stained for CD36 (*green*) and DAPI (*blue*).

using HSA and CD36, we included IgG, but under no condition was IgG seen to bind any FA above ± 10 RU, indicating that FA binding was specific only to HSA and CD36 (Fig. 1*G* shown as representative, other control data not shown).

We then tested whether EA by itself increased Dii-oxLDL uptake and found uptake to be even more pronounced than OA at much lower doses, with doses higher than ~100 μM showing no additional uptake (~R_{max} of Dii-oxLDL uptake). Interestingly, the presence of EA even at lower doses appears to drastically affect the CD36 distribution on the cell surface, especially when compared alongside other FA types (Fig. 5, *a–d*, added alongside other FA representative groups, for comparison).

Oxidized Fatty Acid HODE Does Not Bind CD36 and Does Not Increase Dii-oxLDL Uptake—Because the oxidized FA HODE is the most abundant oxidized FA in oxLDL (29), we used SPR to test whether CD36 could bind HODE. Unexpectedly, we observed dose-responsive binding of HODE with HSA but no binding to CD36 (Fig. 4, *B* and *F*). When HODE was included in the serum-free Dii-oxLDL uptake assay, no increase in Dii-oxLDL uptake was observed in doses up to 100 μM (Fig. 5, *panels e–h*). Doses of HODE above 100 μM were tested but led to a dramatic loss of cytoadherence and no noticeable Dii-oxLDL uptake difference (high dose data not shown; low *n* per microscopy field).

Saturated Fatty Acid Palmitic Acid Binds CD36 and Increases Dii-oxLDL Uptake, Whereas the Polyunsaturated DHA Binds CD36 but Does Not Increase Dii-oxLDL Uptake—To investigate other physiologically important FA classes, we selected saturated PA and polyunsaturated DHA for SPR and Dii-oxLDL uptake studies. We found that CD36 bound both DHA and PA, with particularly high binding responses with DHA before reaching saturating doses (Fig. 4*H*).

Despite the high binding response of DHA with CD36, DHA did not increase Dii-oxLDL uptake, even at the high dose of 500 μM DHA in serum-free medium (Fig. 5, *panels m–p*). This suggests that DHA is binding CD36 while inhibiting oxLDL uptake,

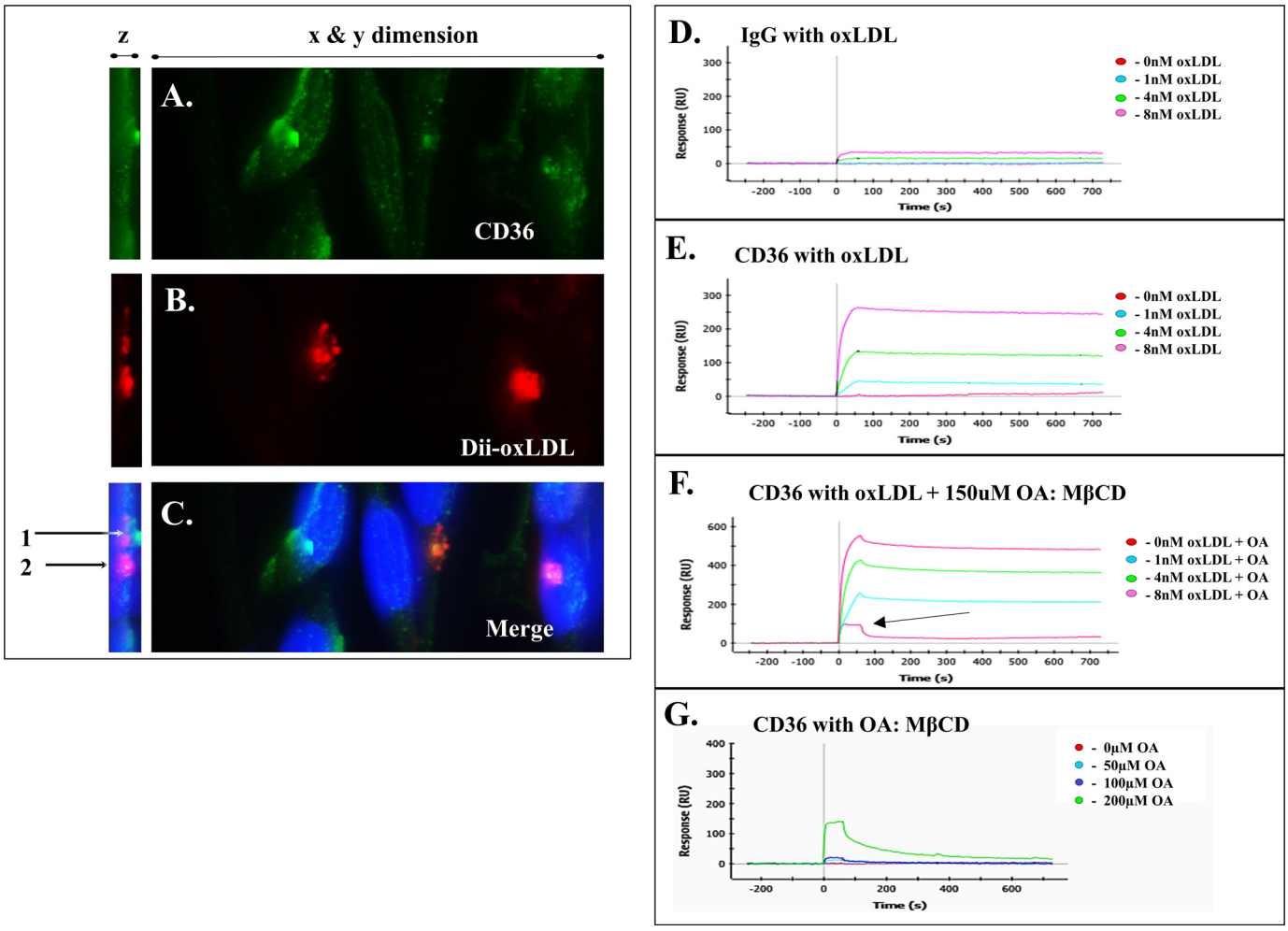

FIGURE 3. *A* and *B*, representative confocal micrograph, including three-dimensional z-stack plane (left edge of each image) at 60× magnification, of HEK293 cells transfected with GFP-CD36 (*A*, *green*), with 5 μg/ml Dii-oxLDL (*B*, *red*) added for 90 min at 37 °C in serum-free DMEM containing 100 μM OA:MβCD (1 OA:6 MβCD). The cells were then fixed and stained with nuclear stain DAPI (*C*, *blue* in the merged image). The *small yellow regions* in the merged image indicate colocalization of EGFP-CD36 and Dii-oxLDL. In the merged image, *arrow 1* illustrates CD36 (*green*) localized on the cell surface, and *arrow 2* indicates Dii-oxLDL and CD36 (*yellow*/*red*) taken into the cell at the nuclear level, indicating uptake rather than cell surface binding. *D* is negative control IgG bound to a GLM SPR chip, whereas *E–G* show CD36 bound to a GLM chip with comparable RU amounts to IgG bound. For *E* and *F*, doses of 0, 1, 4, and 8 nM of oxLDL were pulsed for 60s in PBS, followed by a PBS wash without Dii-oxLDL. In *F*, 150 μM OA:MβCD (1 OA:6 MβCD) was added to each dose of Dii-oxLDL. *G* is from Fig. 1*F*, to contrast the effects of OA:MβCD added without oxLDL. Similarly, in *F*, the *arrow* highlights the 0 nM oxLDL dose and a binding response caused by the presence of 150 μM OA:MβCD. In each panel, note the difference in scale. Also note the RU change from oxLDL alone in *E* is ~30, ~130, and ~250 for 1, 4, and 8 nM oxLDL, respectively. With OA:MβCD, an additional ~100 RU is expected, but instead RU change in *F* is ~200, ~400, and ~500 for 1, 4, and 8 nM, respectively. *D*, only slight binding of oxLDL was observed with IgG bound to the chip. Significant binding of oxLDL is seen with CD36 (*B*); $K_a = 1.0\ e^3$ 1/ms, $K_d = 1.7\ e^{-4}$ 1/s, and $K_D = 1.7\ e^{-7}$ M. Increased binding of oxLDL is seen with CD36 with 150 μM OA present (*C*); $K_a = 1.0\ e^3$ 1/ms, $K_d = 4.4\ e^{-4}$ 1/s, and $K_D = 4.4\ e^{-7}$ m. As with SPR and FA, these numbers may not represent accurate K_D values, but the relative value is important.

which is consistent with other studies showing DHA decreases oxLDL uptake (46).

Furthermore, whereas PA showed binding saturation to CD36 at relatively low doses on SPR compared with other FA classes that were investigated (Fig. 4*G*), PA increased Dii-oxLDL uptake with dose saturation comparable with OA (saturation at ~500 μM PA), while again appearing to change the CD36 surface distribution at higher doses (Fig. 5, *panels i–l*, and data not shown).

CD36 Binds oxLDL Independently of Its Disulfide Bonds—In extended studies to gain insight into localizing FA and oxLDL binding on CD36, we performed a recombinant CD36 Dii-oxLDL binding assay, previously applied to study CD36 binding to various modified forms of LDL, including oxLDL (35). However, we included a heretofore uncharacterized disulfide bond reduction of CD36, employing both the commonly used reducing agent DTT, as well as TCEP. TCEP has the advantage of being a more powerful reducing agent, is considered irreversible by leaving two free cysteines, and, most importantly, TCEP does not reduce metals such as Ni-NTA, used here to immobilize CD36-His_6.

Even under strong reducing conditions, no difference in Dii-oxLDL binding to CD36 was observed (Fig. 6), indicating that the CD36 disulfides are not required for oxLDL binding and may not be a useful drug target for potentially inhibiting oxLDL uptake by CD36. Additionally, our K_D ($K_D = K_a/K_d$) values for each of the three conditions (~25 μg/ml ± ~8) were similar to previously published values for oxLDL binding CD36-His_{12} ($K_D = 10.44 \pm 0.08$ μg/ml (35)), despite our use of dodecyl-β-maltoside in place of octylglucoside in the ligand binding buffer

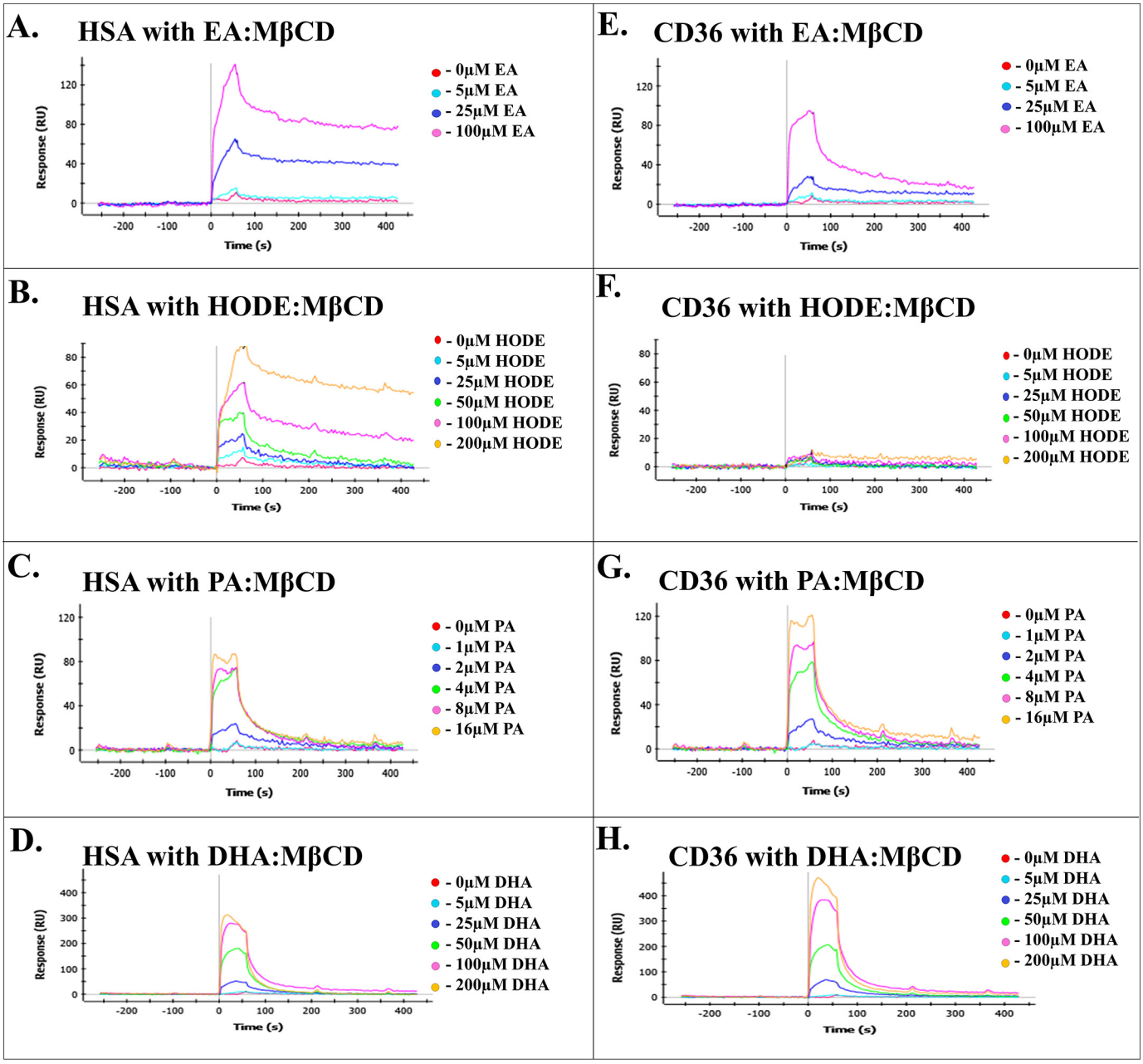

FIGURE 4. *A–D* show HSA bound to a GLM SPR chip. *E–H* show CD36 bound to a GLM chip in the same RU amount as HSA. All wells were normalized to the empty well to correct for nonspecific binding, and none of these FA showed significant binding to IgG (data not shown). *A*, binding of EA is seen with HSA; $K_a = 1.0\ e^3$ 1/ms, $K_d = 1.8\ e^{-3}$ 1/s, and $K_D = 1.8\ e^{-6}$ M. *E*, binding of EA is seen with CD36; $K_a = 1.0\ e^3$ 1/msy, $K_d = 5.1\ e^{-3}$ 1/s, and $K_D = 5.1\ e^{-6}$ M. *B*, binding of HODE is seen with HSA; $K_a = 1.0\ e^3$ 1/ms, $K_d = 6.7\ e^{-3}$ 1/s, and $K_D = 6.7\ e^{-6}$ M. F. No significant binding of HODE to CD36 was seen. *C*, binding of PA is seen with HSA; $K_a = 1.0\ e^3$ 1/ms, $K_d = 1.2\ e^{-2}$ 1/s, and $K_D = 1.2\ e^{-5}$ M. *G*, binding of PA is seen with CD36; $K_a = 1.0\ e^3$ 1/ms, $K_d = 1.1\ e^{-2}$ 1/s, and $K_D = 1.1\ e^{-5}$ M. *D*, binding of DHA is seen with HSA; $K_a = 1.0\ e^3$ 1/ms, $K_d = 1.3\ e^{-2}$ 1/s, and $K_D = 1.3\ e^{-5}$ M. *H*, binding of DHA is seen with CD36; $K_a = 1.0\ e^3$ 1/ms, $K_d = 1.2\ e^{-2}$ 1/s, and $K_D = 1.2\ e^{-5}$ M. Note the differences in RU scale. In each experiment, the highest FA dose shown represents at or near saturation (R_{max}). All FA used was complexed to MβCD with 1:6 FA:MβCD, except for PA (1:12) and DHA (1:1).

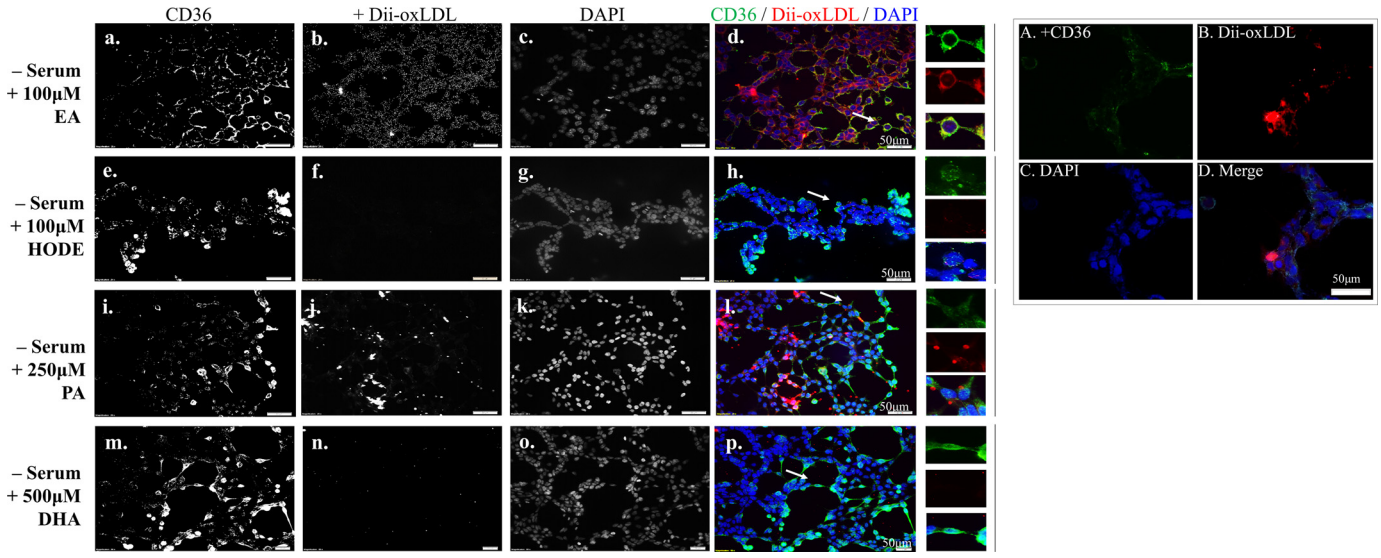

FIGURE 5. *Panels a–p*, merged 20× confocal micrograph of HEK293 cells transfected with CD36, with 5 μg/ml Dii-oxLDL (shown in *red* in the merged image) added for 90 min at 37 °C in serum-free DMEM with 100 μM EA (*panels a–d*) and HODE (*panels e–h*), 250 μM PA (*panels i–l*), and 500 μM DHA (*panels m–p*), all complexed to MβCD as in SPR experiments. Higher doses of HODE were found to abolish cytoadherence, and higher EA doses did not increase Dii-oxLDL uptake (data not shown). PA was found to increase Dii-oxLDL up to ~500 μM (data not shown), similar to the Dii-oxLDL R_{max} when OA was present (Fig. 2*m*-2t). After Dii-oxLDL incubation, the cells were fixed and stained for CD36 (shown in *green* in the merged images) and DAPI (shown in *blue* in the merged images). Significant Dii-oxLDL binding is only seen with added EA (*panels a–d*) and PA (*panels i–l*) but not with HODE (*panels e–h*) or DHA (*panels m–p*). Additionally, CD36 surface distribution changes with each FA (*panels a*, *e*, *i*, and *m*), especially with EA (*panel a*). Furthermore, Dii-oxLDL uptake was substantial and highly diffuse at the cell surface when EA was added (*panel j* and enlarged cell example). *White arrows* in each merged image (*panels d*, *h*, *l*, and *p*) indicate representative enlarged cells in the original color scheme, shown on the *small right panels*. In *A–D*, a similar experiment was performed using serum-free DMEM with 100 μM OA added and 5 μg/ml Dii-oxLDL, along with 24 μM triacsin C for the duration of this 90-min Dii-oxLDL and OA incubation.

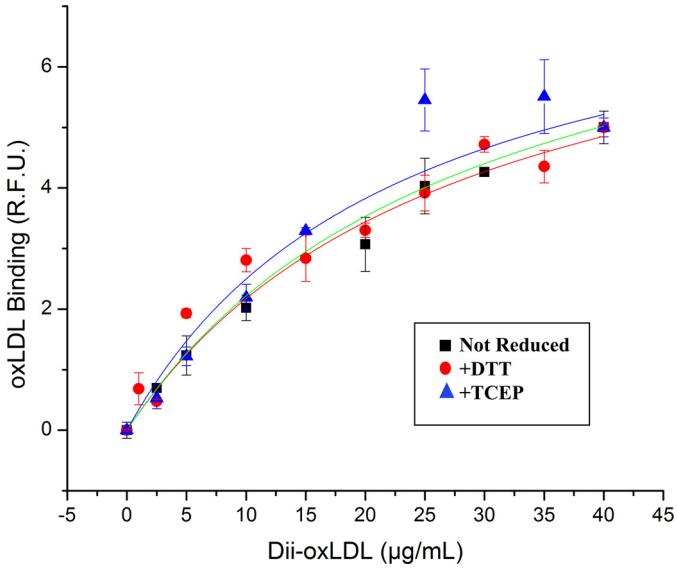

FIGURE 6. **Interaction of CD36 bound to a Ni-NTA-coated plate with Dii-oxLDL added at concentrations of 0, 1, 2. 5, 5, 10, 15, 20, 25, 30, 35, or 40 μg/ml for 90 min at room temperature with no disulfide reduction (*black squares*), 10 mM DTT added (*red circles*), or 10 mM TCEP added (*blue triangles*).** Both DTT and TCEP were added in oxLDL binding buffer for 5 min and then aspirated just prior to adding doses of Dii-oxLDL in oxLDL binding buffer. Binding curves were depicted with relative fluorescence units for ligand binding plotted as a function of ligand concentration. Curve fitting was conducted as described under "Experimental Procedures," from which values for K_D and R_{max} were determined. CD36 with no reduction bound oxLDL with a $K_D = 27.9 \pm 2.1$ μg/ml; $R_{max} = 8.2 \pm 0.3$ μg/ml. CD36 with added DTT bound oxLDL with a $K_D = 29.2 \pm 8.6$ μg/ml; $R_{max} = 8.7 \pm 1.2$ μg/ml. CD36 with added TCEP bound oxLDL with a $K_D = 22.8 \pm 4.6$ μg/ml; $R_{max} = 8.2 \pm 0$ μg/ml. Three independent experiments were performed for each data set.

and the wash buffer. Homology modeling of CD36, based on the crystal structure of family member LIMP2, indicates that the three disulfide bonds of CD36 reside on one "face" of the CD36 protein (15), so we infer that FA and oxLDL bind to CD36 on the other face of its tertiary structure (Fig. 7).

DISCUSSION

Fatty Acid Binding: Novel Findings from Surface Plasmon Resonance—In very recent studies, biophysical approaches have yielded valuable new insights into the structure of CD36 and the molecular interactions of FA analogues in the extracellular region with homology to FABP (15, 47). Throughout the long history of CD36 research, the hypothesis of a single FA binding site has been proposed as a potential mechanism for transport of FA across the plasma membrane into cells (48), as a taste bud sensor of FA (49, 50), and/or as an important site for uptake of oxLDL (51). Our recent study combining biophysics, cell biology, and metabolism in HEK293 cells with and without CD36 led to the finding that although CD36 does not enhance FA transport across the plasma membrane, its presence enhances intracellular triglyceride accumulation (21). New work by other investigators has led to additional evidence of the involvement of a single FA binding site in oxLDL uptake (26).

Here we show that a new approach to study FA binding to CD36 (SPR) yielded the novel finding that the ectodomain of CD36 likely binds several molecules of FA, which could have important ramifications beyond the binding of a single FA molecule for CD36 function. The experimental design (Fig. 1, *Schematic*), including the use of cyclodextrin delivery, permitted quantitative and direct evaluation of the binding of natural FA without the use of high concentrations (up to 1 mM (52)) of nonphysiological probes such as SSO and/or without separation procedures such as column chromatography (*e.g.* Lipidx resin (19)). SPR showed that CD36 binds structurally different long chain FA, including OA, DHA, EA, and PA (monounsatu-

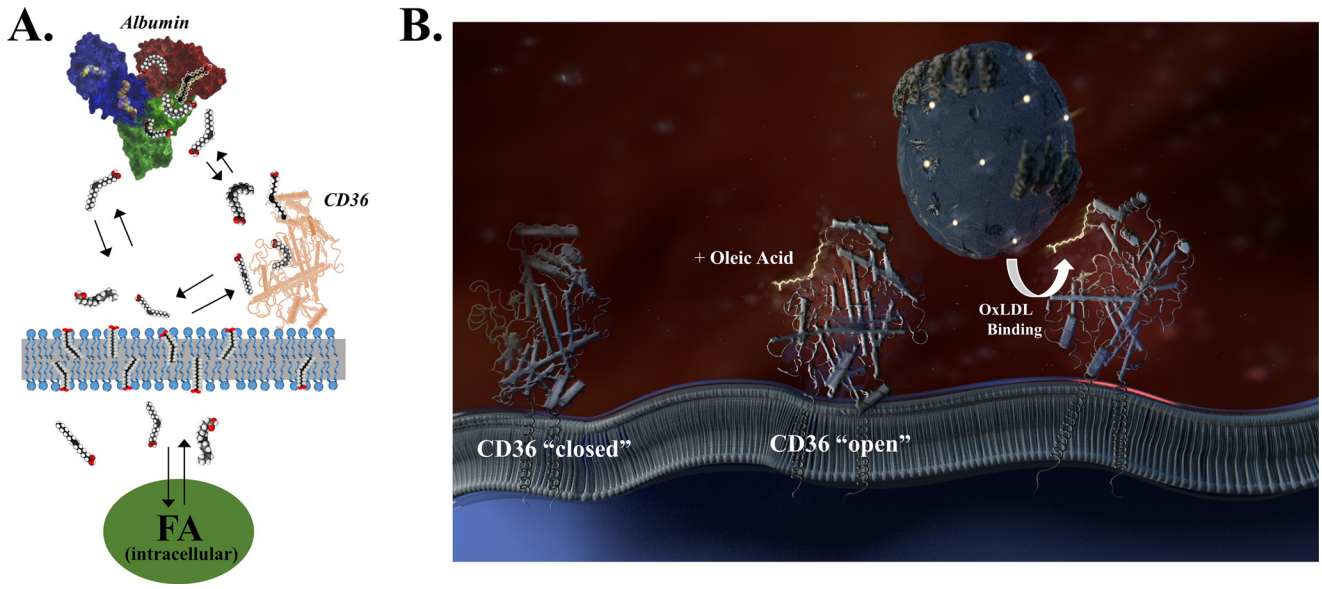

FIGURE 7. *A*, dissociation of long chain FA from albumin and phospholipid bilayers occurs in a time of milliseconds to seconds (33), and we expect generally similar kinetics for the CD36 binding sites, especially with our SPR data. The high abundance of the plasma membrane must be taken in account to determine the partitioning of FA between proteins such as CD36 and the surrounding membrane. *B*, using homology modeling of CD36 from the recently published crystal structure of CD36 family member LIMP-2 (15), we designed this schematic showing a possible mechanism for oxLDL binding, after FA opens the binding site, based on combining our FA binding studies (SPR) and Dii-oxLDL binding/uptake data (microscopy). The site of FA and oxLDL binding is presumably on the opposite face of the CD36 protein structure (*left side*, because the CD36 protein is oriented in the schematic) from the disulfide bond-rich region (*right side*), because we found disulfide bond reduction does not alter oxLDL binding. LDL is shown in the upper background with a single apolipoprotein B-100 wrapping the particle, and *white dots* on the LDL indicate oxidation. One of the implications of the newly characterized FA sites on CD36 is that as the concentration of FA in the plasma and/or plasma membrane increases, the sites on CD36 will have high occupancy, further increasing oxLDL binding and uptake. The figure is not drawn to scale.

TABLE 1

A summary of the FA we tested that bound CD36

Plus signs indicate binding of the FA to CD36. Similarly, uptake of Dii-oxLDL in live HEK293 cells is indicated with plus sign. In general, when a FA bound CD36, uptake of Dii-oxLDL ensued, except for DHA. HODE showed no binding (−) and no enhancement of oxLDL uptake (−).

Fatty acid	CD36 binding	Increased oxLDL uptake
Oleic acid	+	+
9(*S*)-HODE	−	−
Elaidic acid	+	+
Palmitic acid	+	+
DHA	+	−

rated FA, polyunsaturated FA, *trans*-FA, and saturated FA, respectively), but not the oxidized FA HODE. Moreover, the FA binding was dose-dependent and exhibited affinities similar to those of FA on HSA, as measured in parallel experiments by SPR and in agreement with previously measured values (25). The RU values indicate different apparent affinities/saturation of the CD36 binding site(s): PA (~10 μM), EA (~100 μM), DHA (~150 μM), and OA (~200 μM), whereas the very low RU for HODE indicates no significant binding (Table 1).

In comparison with CD36, FA interactions with albumin have been characterized in detail by many biophysical methods, including NMR spectroscopy and x-ray crystallography approaches (40). Nine individual sites on HSA have been recently been detected by two-dimensional NMR, and several NMR peaks were correlated with crystallographic sites well characterized for long chain FA (39). Binding constants measured by two-dimensional NMR on a site-specific basis varied only by a factor of 10 between the highest and lowest affinity sites, with affinity constant (K_D) values similar to those reported by earlier studies (note: $K_D = K_d/K_a$ with units of M) (25, 39).

The high affinity FA binding to CD36 has the important implication that binding at some or all sites could affect protein conformation. The similarity of the kinetics of dissociation of FA from albumin and CD36 observed in our experiments carries the implication that FA have a long enough residency time to have effects on protein structure but also a short enough residency time to allow rapid equilibration between the surrounding aqueous environment, the plasma membrane, and albumin in the plasma (Fig. 7*A*). By contrast, low affinity binding with weak interactions, as suggested by some previous studies (19), would not likely affect protein structure and function or equilibration among the different pools of FA. Furthermore, the amount of FA bound (mol/mol of CD36) could alter protein conformation (Fig. 7*B*), as has been observed for HSA (40), and the apparent bi-phasic binding curve, seen with EA especially, indicates that this is the case. Thus, the existence of these multiple sites could provide a stronger sensor for extracellular and membrane-bound FA concentrations than would a single site.

Effects of Fatty Acid on oxLDL Uptake by CD36—To study effects of FA on CD36-mediated uptake of oxLDL, we utilized our HEK293 cell line designed to express CD36 in the glycosylated form at levels comparable with its endogenous expression in adipocytes (21). As with our previous studies of CD36-mediated uptake of FA, HEK293 cells offered advantages of low or absent endogenous expression of other purported FA transporters (including CD36) (21) and slow metabolism of exogenous FA (53), which permitted focus on mechanisms related to CD36. For the present study, these HEK293 cells are also advantageous because they lack multiple scavenger receptors found on adipocytes and most other cell types, as recognized in other studies using HEK293 cells (54, 55). Our rationale is further

supported by the complication that uptake of modified lipoproteins by scavenger receptors is thought to be central to foam cell formation (56), which has previously been observed to occur over a relatively long time period (1–3 h) (55) and could confound our observation of binding and internalization of oxLDL.

Studies of cells are also complicated because FA bind to the lipid bilayer, and most of the added FA may bind (partition) to the plasma membrane surrounding CD36 (Fig. 7*A*). The presence of the cell membrane must be considered in interpreting the effects of added FA on CD36-mediated uptake of oxLDL. The rapid dissociation of FA from the lipid bilayer and plasma albumin will permit binding to sites on CD36 by equilibration, as illustrated in Fig. 7*A*. We can assume that FA entering the membrane (even from an intracellular origin) or in the proximity of the membrane will bind to sites on CD36, and we can predict that higher concentrations of FA will lead to greater occupancy of CD36 sites. Furthermore, from our cell-free binding studies with SPR, we can predict that effects of FA on CD36 might be differentiated from nonspecific effects by dependence on the FA structure.

Our major findings in our HEK293 cells are that: (i) oxLDL uptake was limited in serum-free medium without added FA and in charcoal-stripped FA-depleted serum; (ii) addition of exogenous OA to serum-free medium enhanced oxLDL uptake to a level observed with serum; (iii) PA and EA also enhanced oxLDL in a dose-dependent manner; (iv) DHA did not enhance CD36-mediated uptake of oxLDL, although it bound to CD36 in our SPR assay; and (v) HODE did not enhance uptake of oxLDL and did not bind to CD36 in our SPR assay. These findings are summarized in Table 1.

The work presented is the first systematic study of the effects of FA together with oxLDL on CD36. Although published results to date from other groups have used similar assays with labeled oxLDL in cells expressing CD36, they have not shown dependence of oxLDL binding upon serum and/or FA. This is likely due to different experimental conditions and because the studies were not comprehensive. For example, other studies have used monocyte-like or macrophage-like cell lines that express other compensating oxLDL scavenger receptors that likely bind oxLDL in a FA-independent manner (*e.g.* THP-1 cells (57)). Additionally, compared with our study that used high doses of FA for *in vitro* experiments (up to 500 μM to observe the R_{max} of Dii-oxLDL uptake), physiological FA concentrations range between 250 and 3,000 μM, dependent on factors such as fasting/nutrition state and exercise (58). Lower levels of oxLDL uptake can be seen with highly sensitive oxLDL detection techniques such as radiolabeling (^{125}I-oxLDL) or high magnification/high exposure microscopy to observe oxLDL binding/uptake, coupled with serum-free medium delivery of oxLDL (15, 59, 60). We quantified the differences between Dii-oxLDL uptake using serum-free medium (small levels of uptake), serum-containing medium (large levels of uptake), and increasing doses of FA in serum-free medium (increasing levels of Dii-oxLDL uptake, rescued to serum-containing levels), and we did not observe any unusual cell phenotype changes, in the short time frame of our observation (Fig. 2). Similarly, although OA and PA have been found to increase CD36 surface expression (35), our experimental time scale likely does not allow enough time for increases in surface expression of CD36 to drastically alter oxLDL uptake. However, our finding that CD36 surface distribution was changed using different doses of FA is of interest and an aim in our future work. We additionally utilized ethanol-free delivery of all FA in these assays, namely using MβCD and water, to eliminate possible solvent perturbations in the binding and uptake of Dii-oxLDL.

Implications of Our Uptake Studies for Protein Structure: Disulfide Bonds of CD36—CD36 mediated cytoadherence of *P. falciparum* (malaria)-infected red blood cells is lost following treatment of CD36-expressing cells with the reducing agent DTT (18). This finding indicates therapeutic potential in reducing agents, such as the nontoxic drug *N*-acetylcysteine, to prevent or treat malaria complications caused by infected red blood cell cytoadhesion. However, these same treatment strategies may not be useful in preventing oxLDL binding and internalization through a CD36-dependent mechanism, because we observed that disulfide reduction did not affect Dii-oxLDL binding to CD36 (Fig. 6). This also suggests that the FA and oxLDL binding site on CD36 is not located in the cysteine-rich region that interacts with *P. falciparum*-infected red blood cells, but possibly on the other face of CD36, as represented by the bound OA in Fig. 7*B*.

Evidence for Direct Mechanistic Effects of FA on oxLDL Uptake by CD36—Because CD36 binds and initiates uptake of oxLDL and we found FA to be required for this CD36-dependent mass-transport of oxLDL, we speculate that FA binding alters the protein conformation with functional consequences. The structure LIMP-2 (15) provides a very plausible mechanism for homologous family member CD36 uptake of cholesteryl esters through a hydrophobic groove. oxLDL fits into a large central cavity homologous to the LIMP-2 cavity for glucocerebrosidase. We speculate that CD36 maintains a "closed" conformation to oxLDL binding until a specific FA (*i.e.* OA, EA, and PA) is present. FA binding could shift CD36 into an "open" conformation that is favorable to oxLDL binding (Fig. 7*B*). The one well characterized FA binding site and the oxLDL binding site appear to be in the same region, specifically K164 (26). Binding to this site and other sites could influence oxLDL binding and contribute to opening or closing the binding pocket.

The contribution of direct FA binding enhancement of Dii-oxLDL docking to CD36 is supported by our *in vitro* SPR results, pulsing oxLDL together with OA (Fig. 3, *D–F*). This interpretation is consistent with recent observations that fragments of the CD36 protein on multiwall plates had up to 50% less binding of oxLDL when certain FA (including OA) were present at extremely high (~1 mM) concentrations, levels that outcompete the oxLDL at this (single) oxLDL binding/docking site. Other studies of CD36 binding or "scavenging" diverse lipid ligands also indicate a pH profile and salt concentration dependence, suggestive of an electrostatic mechanism of lipid binding (14). Because the FA in these assays is mainly deprotonated in the extracellular environment (*i.e.* OA pK_a = 9.85, etc. (61)), FA could facilitate oxLDL docking through anionic interactions with CD36. Hydrophobic interactions with the FA acyl chain appear to play a contribution, because the two least hydrophobic FA studied either do not bind to CD36 (HODE) or do not enhance uptake of oxLDL (DHA). Because DHA binds

avidly to CD36 (SPR shows higher binding than to HSA; Fig. 4, *D* and *H*), it could promote an open oxLDL binding conformation on CD36 unfavorable for the binding of oxLDL. This finding agrees with previous data showing that DHA lowers oxLDL uptake (62). Conversely, it is interesting to note that EA is the most abundant *trans*-FA found in atheromatous plaque (63, 64), and we found that EA bound CD36 on SPR and aggressively increased Dii-oxLDL.

Conclusions—Overall, our study provides a novel mechanism of CD36 binding oxLDL, through first binding FA. Our data also indicate that multiple FA binding sites likely exist on CD36 but did not identify specific sites within the protein. Future studies using hydrogen exchange mass spectroscopy with recombinant, full-length CD36 embedded into nanodiscs with added FA are being pursued (65, 66), as well as NMR studies using the soluble CD36 ectodomain. In addition, we recognize that because all FA species studied can partition into the lipid bilayer of the plasma membrane, FA could exert effects on membrane organization, which could also influence oxLDL uptake. We have initiated systematic studies with membrane fluidity probes in our HEK293 cells, with and without CD36, to investigate changes in membrane order with different FA.

The presence of multiple binding sites for FA on CD36 could enhance the sensitivity of CD36 to the concentration of plasma FA. Because obesity and type 2 diabetes are characterized by high plasmas levels of long chain FA (67, 68), the demonstrated enhancement of oxLDL uptake by increases in common dietary FA may contribute to the pathophysiology of these diseases. Our results also support the hypothesis that CD36 may be a link between insulin resistance states from studies showing that increased plasma FA levels were associated with enhanced CD36 expression and increased internalization of oxLDL (69).

The anomalous and intriguing results for DHA and HODE may have implications for cardiovascular disease because oxLDL uptake triggers a signaling response that is pro-inflammatory and pro-atherogenic (7). DHA might inhibit inflammatory responses by binding to CD36 in a manner that inhibits CD36-oxLDL binding. And although human oxLDL often contains significant amounts of HODE (29, 70), HODE did not enhance CD36-mediated uptake of oxLDL, possibly because it does not bind to the ectodomain of CD36. Therefore, other proteins could be affected by HODE, because HODE consumption, in association with a high fat diet, has been shown to increase aortic lesion areas by >100% (62).

Acknowledgments—We thank Michael T. Kirber (Boston University School of Medicine) for technical confocal microscopy assistance, Christopher Jay for graphic design work, and Grace Yee for help in preparation of the manuscript. We thank David A. Harris (Boston University School of Medicine) for use of the surface plasmon resonance machine, Brian R. Fluharty (Boston University School of Medicine) for technical SPR assistance, and Adrian Whitty (Boston University) for SPR expertise and advice.

REFERENCES

1. Moore, K. J., and Freeman, M. W. (2006) Scavenger receptors in atherosclerosis: beyond lipid uptake. *Arterioscler. Thromb. Vasc. Biol.* **26,** 1702–1711
2. Plüddemann, A., Neyen, C., and Gordon, S. (2007) Macrophage scavenger receptors and host-derived ligands. *Methods* **43,** 207–217
3. Murphy, J. E., Tedbury, P. R., Homer-Vanniasinkam, S., Walker, J. H., and Ponnambalam, S. (2005) Biochemistry and cell biology of mammalian scavenger receptors. *Atherosclerosis* **182,** 1–15
4. Ramos-Arellano, L. E., Muñoz-Valle, J. F., De la Cruz-Mosso, U., Salgado-Bernabé, A. B., Castro-Alarcón, N., and Parra-Rojas, I. (2014) Circulating CD36 and oxLDL levels are associated with cardiovascular risk factors in young subjects. *BMC Cardiovasc. Disord.* **14,** 54
5. Dushkin, M. I. (2012) Macrophage/foam cell is an attribute of inflammation: mechanisms of formation and functional role. *Biochemistry* **77,** 327–338
6. Avraham-Davidi, I., Grunspan, M., and Yaniv, K. (2013) Lipid signaling in the endothelium. *Exp. Cell Res.* **319,** 1298–1305
7. Silverstein, R. L., Li, W., Park, Y. M., and Rahaman, S. O. (2010) Mechanisms of cell signaling by the scavenger receptor CD36: implications in atherosclerosis and thrombosis. *Trans. Am. Clin. Climatol Assoc.* **121,** 206–220
8. Maiolino, G., Rossitto, G., Caielli, P., Bisogni, V., Rossi, G. P., and Calò, L. A. (2013) The role of oxidized low-density lipoproteins in atherosclerosis: the myths and the facts. *Mediators Inflamm.* **2013,** 714653
9. de Villiers, W. J., Cai, L., Webb, N. R., de Beer, M. C., van der Westhuyzen, D. R., and de Beer, F. C. (2001) CD36 does not play a direct role in HDL or LDL metabolism. *J. Lipid Res.* **42,** 1231–1238
10. Greaves, D. R., and Gordon, S. (2009) The macrophage scavenger receptor at 30 years of age: current knowledge and future challenges. *J. Lipid Res.* **50,** (suppl.) S282–S286
11. Kashiwagi, H., Tomiyama, Y., Honda, S., Kosugi, S., Shiraga, M., Nagao, N., Sekiguchi, S., Kanayama, Y., Kurata, Y., and Matsuzawa, Y. (1995) Molecular basis of CD36 deficiency. Evidence that a 478C→T substitution (proline90→serine) in CD36 cDNA accounts for CD36 deficiency. *J. Clin. Invest.* **95,** 1040–1046
12. Nozaki, S., Kashiwagi, H., Yamashita, S., Nakagawa, T., Kostner, B., Tomiyama, Y., Nakata, A., Ishigami, M., Miyagawa, J., and Kameda-Takemura, K. (1995) Reduced uptake of oxidized low density lipoproteins in monocyte-derived macrophages from CD36-deficient subjects. *J. Clin. Invest.* **96,** 1859–1865
13. Puente Navazo, M. D., Daviet, L., Ninio, E., and McGregor, J. L. (1996) Identification on human CD36 of a domain (155–183) implicated in binding oxidized low-density lipoproteins (Ox-LDL). *Arterioscler. Thromb. Vasc. Biol.* **16,** 1033–1039
14. Kar, N. S., Ashraf, M. Z., Valiyaveettil, M., and Podrez, E. A. (2008) Mapping and characterization of the binding site for specific oxidized phospholipids and oxidized low density lipoprotein of scavenger receptor CD36. *J. Biol. Chem.* **283,** 8765–8771
15. Neculai, D., Schwake, M., Ravichandran, M., Zunke, F., Collins, R. F., Peters, J., Neculai, M., Plumb, J., Loppnau, P., Pizarro, J. C., Seitova, A., Trimble, W. S., Saftig, P., Grinstein, S., and Dhe-Paganon, S. (2013) Structure of LIMP-2 provides functional insights with implications for SR-BI and CD36. *Nature* **504,** 172–176
16. Martínez, V. G., Moestrup, S. K., Holmskov, U., Mollenhauer, J., and Lozano, F. (2011) The conserved scavenger receptor cysteine-rich superfamily in therapy and diagnosis. *Pharmacol. Rev.* **63,** 967–1000
17. Rasmussen, J. T., Berglund, L., Rasmussen, M. S., and Petersen, T. E. (1998) Assignment of disulfide bridges in bovine CD36. *Eur. J. Biochem.* **257,** 488–494
18. Gruarin, P., Primo, L., Ferrandi, C., Bussolino, F., Tandon, N. N., Arese, P., Ulliers, D., and Alessio, M. (2001) Cytoadherence of *Plasmodium falciparum*-infected erythrocytes is mediated by a redox-dependent conformational fraction of CD36. *J. Immunol.* **167,** 6510–6517
19. Baillie, A. G., Coburn, C. T., and Abumrad, N. A. (1996) Reversible binding of long-chain fatty acids to purified FAT, the adipose CD36 homolog. *J. Membr. Biol.* **153,** 75–81
20. Su, X., and Abumrad, N. A. (2009) Cellular fatty acid uptake: a pathway under construction. *Trends Endocrinol. Metab.* **20,** 72–77
21. Xu, S., Jay, A., Brunaldi, K., Huang, N., and Hamilton, J. A. (2013) CD36 enhances fatty acid uptake by increasing the rate of intracellular esterification but not transport across the plasma membrane. *Biochemistry* **52,**

7254–7261
22. Krammer, J., Digel, M., Ehehalt, F., Stremmel, W., Füllekrug, J., and Ehehalt, R. (2011) Overexpression of CD36 and acyl-CoA synthetases FATP2, FATP4 and ACSL1 increases fatty acid uptake in human hepatoma cells. *Int. J. Med. Sci.* **8,** 599–614
23. Harmon, C. M., Luce, P., Beth, A. H., and Abumrad, N. A. (1991) Labeling of adipocyte membranes by sulfo-*N*-succinimidyl derivatives of long-chain fatty acids: inhibition of fatty acid transport. *J. Membr. Biol.* **121,** 261–268
24. Harmon, C. M., and Abumrad, N. A. (1993) Binding of sulfosuccinimidyl fatty acids to adipocyte membrane proteins: isolation and amino-terminal sequence of an 88-kD protein implicated in transport of long-chain fatty acids. *J. Membr. Biol.* **133,** 43–49
25. Spector, A. A. (1975) Fatty acid binding to plasma albumin. *J. Lipid Res.* **16,** 165–179
26. Kuda, O., Pietka, T. A., Demianova, Z., Kudova, E., Cvacka, J., Kopecky, J., and Abumrad, N. A. (2013) Sulfo-*N*-succinimidyl oleate (SSO) inhibits fatty acid uptake and signaling for intracellular calcium via binding CD36 lysine 164: SSO also inhibits oxidized low density lipoprotein uptake by macrophages. *J. Biol. Chem.* **288,** 15547–15555
27. Takai, M., Kozai, Y., Tsuzuki, S., Matsuno, Y., Fujioka, M., Kamei, K., Inagaki, H., Eguchi, A., Matsumura, S., Inoue, K., and Fushiki, T. (2014) Unsaturated long-chain fatty acids inhibit the binding of oxidized low-density lipoproteins to a model CD36. *Biosci. Biotechnol. Biochem.* **78,** 238–244
28. Kozai, Y., Tsuzuki, S., Takai, M., Eguchi, A., Matsumura, S., Inoue, K., and Fushiki, T. (2014) Further validation of unsaturated long-chain fatty acids as inhibitors for oxidized low-density lipoprotein binding to CD36 via assays with synthetic CD36 peptide-cross-linked plates. *Biosci. Biotechnol. Biochem.* **78,** 839–842
29. Folcik, V. A., and Cathcart, M. K. (1994) Predominance of esterified hydroperoxy-linoleic acid in human monocyte-oxidized LDL. *J. Lipid Res.* **35,** 1570–1582
30. Yaney, G. C., Civelek, V. N., Richard, A. M., Dillon, J. S., Deeney, J. T., Hamilton, J. A., Korchak, H. M., Tornheim, K., Corkey, B. E., and Boyd, A. E., 3rd. (2001) Glucagon-like peptide 1 stimulates lipolysis in clonal pancreatic beta-cells (HIT). *Diabetes* **50,** 56–62
31. Byun, J., Verardo, M. R., Sumengen, B., Lewis, G. P., Manjunath, B. S., and Fisher, S. K. (2006) Automated tool for the detection of cell nuclei in digital microscopic images: application to retinal images. *Mol. Vis.* **12,** 949–960
32. McDonnell, J. M. (2001) Surface plasmon resonance: towards an understanding of the mechanisms of biological molecular recognition. *Curr. Opin. Chem. Biol.* **5,** 572–577
33. Zhang, F., Kamp, F., and Hamilton, J. A. (1996) Dissociation of long and very long chain fatty acids from phospholipid bilayers. *Biochemistry* **35,** 16055–16060
34. Crouse, J. R., Parks, J. S., Schey, H. M., and Kahl, F. R. (1985) Studies of low density lipoprotein molecular weight in human beings with coronary artery disease. *J. Lipid Res.* **26,** 566–574
35. Martin, C. A., Longman, E., Wooding, C., Hoosdally, S. J., Ali, S., Aitman, T. J., Gutmann, D. A., Freemont, P. S., Byrne, B., and Linton, K. J. (2007) Cd36, a class B scavenger receptor, functions as a monomer to bind acetylated and oxidized low-density lipoproteins. *Protein Sci.* **16,** 2531–2541
36. Hoosdally, S. J., Andress, E. J., Wooding, C., Martin, C. A., and Linton, K. J. (2009) The Human Scavenger Receptor CD36: glycosylation status and its role in trafficking and function. *J. Biol. Chem.* **284,** 16277–16288
37. Brunaldi, K., Huang, N., and Hamilton, J. A. (2010) Fatty acids are rapidly delivered to and extracted from membranes by methyl-β-cyclodextrin. *J. Lipid Res.* **51,** 120–131
38. Pillai, B. K., Jasuja, R., Simard, J. R., and Hamilton, J. A. (2009) Fast diffusion of very long chain saturated fatty acids across a bilayer membrane and their rapid extraction by cyclodextrins: implications for adrenoleukodystrophy. *J. Biol. Chem.* **284,** 33296–33304
39. Krenzel, E. S., Chen, Z., and Hamilton, J. A. (2013) Correspondence of fatty acid and drug binding sites on human serum albumin: a two-dimensional nuclear magnetic resonance study. *Biochemistry* **52,** 1559–1567
40. Hamilton, J. A. (2013) NMR reveals molecular interactions and dynamics of fatty acid binding to albumin. *Biochim. Biophys. Acta* **1830,** 5418–5426
41. Zhang, F., Lücke, C., Baier, L. J., Sacchettini, J. C., and Hamilton, J. A. (1997) Solution structure of human intestinal fatty acid binding protein: implications for ligand entry and exit. *J. Biomol. NMR* **9,** 213–228
42. Cai, J., Lücke, C., Chen, Z., Qiao, Y., Klimtchuk, E., and Hamilton, J. A. (2012) Solution structure and backbone dynamics of human liver fatty acid binding protein: fatty acid binding revisited. *Biophys. J.* **102,** 2585–2594
43. Abumrad, N., Coburn, C., and Ibrahimi, A. (1999) Membrane proteins implicated in long-chain fatty acid uptake by mammalian cells: CD36, FATP and FABPm. *Biochim. Biophys. Acta* **1441,** 4–13
44. Gaubatz, J. W., Gillard, B. K., Massey, J. B., Hoogeveen, R. C., Huang, M., Lloyd, E. E., Raya, J. L., Yang, C. Y., and Pownall, H. J. (2007) Dynamics of dense electronegative low density lipoproteins and their preferential association with lipoprotein phospholipase A_2. *J. Lipid Res.* **48,** 348–357
45. Stoll, L. L., and Spector, A. A. (1984) Changes in serum influence the fatty acid composition of established cell lines. *In Vitro.* **20,** 732–738
46. Madonna, R., Salerni, S., Schiavone, D., Glatz, J. F., Geng, Y. J., and De Caterina, R. (2011) Omega-3 fatty acids attenuate constitutive and insulin-induced CD36 expression through a suppression of PPAR α/γ activity in microvascular endothelial cells. *Thromb. Haemost.* **106,** 500–510
47. Tarhda, Z., Semlali, O., Kettani, A., Moussa, A., Abumrad, N. A., and Ibrahimi, A. (2013) Three dimensional structure prediction of fatty acid binding site on human transmembrane receptor CD36. *Bioinform. Biol. Insights* **7,** 369–373
48. Pownall, H., and Moore, K. (2014) Commentary on fatty acid wars: the diffusionists versus the translocatists. *Arterioscler. Thromb. Vasc. Biol.* **34,** e8–e9
49. Le Foll, C., Dunn-Meynell, A., Musatov, S., Magnan, C., and Levin, B. E. (2013) FAT/CD36: a major regulator of neuronal fatty acid sensing and energy homeostasis in rats and mice. *Diabetes* **62,** 2709–2716
50. Degrace-Passilly, P., and Besnard, P. (2012) CD36 and taste of fat. *Curr. Opin. Clin. Nutr. Metab. Care* **15,** 107–111
51. Silverstein, R. L. (2009) Inflammation, atherosclerosis, and arterial thrombosis: role of the scavenger receptor CD36. *Cleve. Clin. J. Med.* **76,** S27–S30
52. Harmon, C. M., Luce, P., and Abumrad, N. A. (1992) Labelling of an 88 kDa adipocyte membrane protein by sulpho-*N*-succinimidyl long-chain fatty acids: inhibition of fatty acid transport. *Biochem. Soc. Trans.* **20,** 811–813
53. Simard, J. R., Meshulam, T., Pillai, B. K., Kirber, M. T., Brunaldi, K., Xu, S., Pilch, P. F., and Hamilton, J. A. (2010) Caveolins sequester FA on the cytoplasmic leaflet of the plasma membrane, augment triglyceride formation, and protect cells from lipotoxicity. *J. Lipid Res.* **51,** 914–922
54. Robbins, A. K., and Horlick, R. A. (1998) Macrophage scavenger receptor confers an adherent phenotype to cells in culture. *BioTechniques* **25,** 240–244
55. Baranova, I. N., Vishnyakova, T. G., Bocharov, A. V., Leelahavanichkul, A., Kurlander, R., Chen, Z., Souza, A. C., Yuen, P. S., Star, R. A., Csako, G., Patterson, A. P., and Eggerman, T. L. (2012) Class B scavenger receptor types I and II and CD36 mediate bacterial recognition and proinflammatory signaling induced by *Escherichia coli*, lipopolysaccharide, and cytosolic chaperonin 60. *J. Immunol.* **188,** 1371–1380
56. Hofnagel, O., Luechtenborg, B., Weissen-Plenz, G., and Robenek, H. (2007) Statins and foam cell formation: impact on LDL oxidation and uptake of oxidized lipoproteins via scavenger receptors. *Biochim. Biophys. Acta* **1771,** 1117–1124
57. Amézaga, N., Sanjurjo, L., Julve, J., Aran, G., Pérez-Cabezas, B., Bastos-Amador, P., Armengol, C., Vilella, R., Escolà-Gil, J. C., Blanco-Vaca, F., Borràs, F. E., Valledor, A. F., and Sarrias, M. R. (2014) Human scavenger protein AIM increases foam cell formation and CD36-mediated oxLDL uptake. *J. Leukocyte Biol.* **95,** 509–520
58. Gerich, J. E., Langlois, M., Schneider, V., Karam, J. H., and Noacco, C. (1974) Effects of alternations of plasma free fatty acid levels on pancreatic glucagon secretion in man. *J. Clin. Invest.* **53,** 1284–1289
59. Sun, B., Boyanovsky, B. B., Connelly, M. A., Shridas, P., van der Westhuyzen, D. R., and Webb, N. R. (2007) Distinct mechanisms for OxLDL uptake and cellular trafficking by class B scavenger receptors CD36 and SR-BI. *J. Lipid Res.* **48,** 2560–2570

60. Sun, B., Eckhardt, E. R., Shetty, S., van der Westhuyzen, D. R., and Webb, N. R. (2006) Quantitative analysis of SR-BI-dependent HDL retroendocytosis in hepatocytes and fibroblasts. *J. Lipid Res.* **47,** 1700–1713
61. Kanicky, J. R., and Shah, D. O. (2002) Effect of degree, type, and position of unsaturation on the pKa of long-chain fatty acids. *J. Colloid Interface Sci.* **256,** 201–207
62. Khan-Merchant, N., Penumetcha, M., Meilhac, O., and Parthasarathy, S. (2002) Oxidized fatty acids promote atherosclerosis only in the presence of dietary cholesterol in low-density lipoprotein receptor knockout mice. *J. Nutr.* **132,** 3256–3262
63. Bassett, C. M., Edel, A. L., Patenaude, A. F., McCullough, R. S., Blackwood, D. P., Chouinard, P. Y., Paquin, P., Lamarche, B., and Pierce, G. N. (2010) Dietary vaccenic acid has antiatherogenic effects in LDLr$^{-/-}$ mice. *J. Nutr.* **140,** 18–24
64. Stachowska, E., Dolegowska, B., Chlubek, D., Wesolowska, T., Ciechanowski, K., Gutowski, P., Szumilowicz, H., and Turowski, R. (2004) Dietary trans fatty acids and composition of human atheromatous plaques. *Eur. J. Nutr.* **43,** 313–318
65. Sáez-Cirión, A., and Nieva, J. L. (2002) Conformational transitions of membrane-bound HIV-1 fusion peptide. *Biochim. Biophys. Acta* **1564,** 57–65
66. Hebling, C. M., Morgan, C. R., Stafford, D. W., Jorgenson, J. W., Rand, K. D., and Engen, J. R. (2010) Conformational analysis of membrane proteins in phospholipid bilayer nanodiscs by hydrogen exchange mass spectrometry. *Anal. Chem.* **82,** 5415–5419
67. Ebbert, J. O., and Jensen, M. D. (2013) Fat depots, free fatty acids, and dyslipidemia. *Nutrients* **5,** 498–508
68. Mittendorfer, B., Magkos, F., Fabbrini, E., Mohammed, B. S., and Klein, S. (2009) Relationship between body fat mass and free fatty acid kinetics in men and women. *Obesity* **17,** 1872–1877
69. Kashyap, S. R., Ioachimescu, A. G., Gornik, H. L., Gopan, T., Davidson, M. B., Makdissi, A., Major, J., Febbraio, M., and Silverstein, R. L. (2009) Lipid-induced insulin resistance is associated with increased monocyte expression of scavenger receptor CD36 and internalization of oxidized LDL. *Obesity* **17,** 2142–2148
70. Ku, G., Thomas, C. E., Akeson, A. L., and Jackson, R. L. (1992) Induction of interleukin 1β expression from human peripheral blood monocyte-derived macrophages by 9-hydroxyoctadecadienoic acid. *J. Biol. Chem.* **267,** 14183–14188